Earth Syst. Dynam. Discuss., 6, 2273–2322, 2015
www.earth-syst-dynam-discuss.net/6/2273/2015/
doi:10.5194/esdd-6-2273-2015

Earth System Dynamics Discussions
Open Access
EGU

Severe summer heat waves over Georgia: trends, patterns and driving forces

I. Keggenhoff[1], **M. Elizbarashvili**[2], **and L. King**[1]

[1]Justus Liebig University Giessen, Department of Geography, Giessen, Germany
[2]Ivane Javakhishvili Tbilisi State University, Department of Geography, Tbilisi, Georgia

Received: 21 October 2015 – Accepted: 27 October 2015 – Published: 9 November 2015

Correspondence to: I. Keggenhoff (ina.keggenhoff@geogr.uni-giessen.de)

Published by Copernicus Publications on behalf of the European Geosciences Union.

Abstract

During the last 50 years Georgia experienced a rising number of severe summer heat waves causing increasing heat-health impacts. In this study, the 10 most severe heat waves between 1961 and 2010 and recent changes in heat wave characteristics have been detected from 22 homogenized temperature minimum and maximum series using the Excess Heat Factor (EHF). A composite and Canonical Correlation Analysis (CCA) have been performed to study summer heat wave patterns and their relationships to the selected predictors: mean Sea Level Pressure (SLP), Geopotential Height at 500 mb (Z500), Sea Surface Temperature (SST), Zonal (u-wind500) and Meridional Wind at 500 mb (v-wind500), Vertical Velocity at 500 mb (O500), Outgoing Longwave Radiation (OLR), Relative Humidity (RH500), Precipitation (RR) and Soil Moisture (SM). Most severe heat events during the last 50 years are identified in 2007, 2006 and 1998. Largest significant trend magnitudes for the number, intensity and duration of low and high-impact heat waves have been found during the last 30 years. Significant changes in the heat wave predictors reveal that all relevant surface and atmospheric patterns contributing to heat waves have been intensified between 1961 and 2010. Composite anomalies and CCA patterns provide evidence of a large anticyclonic blocking pattern over the southern Ural Mountains, which attracts warm air masses from the Southwest, enhances subsidence and surface heating, shifts the African Intertropical Convergence Zone (ITCZ) northwards, and causes a northward shift of the subtropical jet. Moreover, pronounced precipitation and soil moisture deficiency throughout Georgia contribute to the heat wave formation and persistence over Georgia. Due to different large- to mesoscale circulation patterns and the local terrain, heat wave effects over Eastern Georgia are dominated by subsidence and surface heating, while convective rainfall and cooling are observed in the West.

ESDD
6, 2273–2322, 2015

1 Introduction

Anthropogenic influences on climate since the mid-20th century resulted in a change of frequency and intensity of daily temperature extremes and doubled the probability of occurrence of heat waves in some regions of the world (Beniston and Stephenson, 2004; Stott et al., 2004; Jones et al., 2008; Christidis et al., 2011, 2012; IPCC, 2014). The fact that the global averaged heat waves are projected to increase in frequency, intensity and duration (Meehl and Tebaldi, 2004; Perkins et al., 2012) makes it important to investigate their driving mechanisms with special regards to large-scale atmospheric circulation, land–sea interactions and regional processes.

Heat wave patterns in Georgia are highly dependent on the large scale synoptic, thermic patterns and the local terrain. Temperature tends to increase eastwards with increasing continentality in combination with a decrease in precipitation. The Stavropol upland in the Caucasus Foreland and the Surami Ridge in Transcaucasia form important climatic divides. The air, advected by depressions from the Black Sea, loses most of its moisture over the Colchis lowland and, having crossed the Surami Ridge, descends in the Kura lowland as a dry airflow. The summer circulation patterns over Georgia are influenced by a subtropical high pressure in the west and the Asian depression in the east (Ziv et al., 2004; de Vries et al., 2013). The lower levels are dominated by the so-called “Red Sea trough” and the “Persian trough”, surface low-pressure troughs that extends from the Asian monsoon across the Red Sea and Persian Gulf to southern Turkey (Fig. 1a). As a result of the Red Sea and Persian trough and the subtropical anticyclone of the Atlantic (Azores), northwesterly winds blow over the Black Sea. In accordance with Arkhipkin et al. (2014, 2015) these winds yield a continual cool advection from Eastern Europe, as seen in the average wind fields (Fig. 1b). In addition, Georgia is dominated by summer convection centered over the Armenian-Dzavakhetian volcanic plateau as shown in the low vertical pressure velocity field (Fig. 1c). The Greater and Southern Caucasus block northwesterly winds from the East European plain and

ESDD
6, 2273–2322, 2015

orographic convection is induced followed by low to heavy precipitation events at the windward slopes of the high mountain ridges.

The Caucasus represents one of world's hot spots most vulnerable to climate change (Shahgedanova, 2002). According to findings by Keggenhoff et al. (2014) Georgia experienced pronounced warming trends in temperature extremes and a decrease in wet days ($R \geq 1$ mm) during 1971 and 2010. Since 1960s, monthly minimum and maximum temperature increased by 0.22 and 0.36 °C, respectively, while warm extremes show larger trends than cold extremes. The trend for warm spells was observed to be significantly increasing by 1.7 days (Keggenhoff et al., 2015a). Future climate extreme projections by Lieferheld et al. (2012, 2013) show a pronounced increase in summer temperature projected by the end of the 21st century (relative to the 1961–1990 period), especially for temperature maxima (by over 6 °C) over the western part of Georgia. The number of dry days will increase significantly in Eastern Georgia between the projection period 2040 to 2069. However, for Western Georgia a negative trend for the number of dry days is projected.

Heat waves are among the most threatening meteorological hazards related to global warming posing impacts to society, economy and ecology. Heat-related morbidity and mortality in Georgia is expected to increase due to significant positive trends in the intensity, frequency and duration of heat waves during the last 50 years (Keggenhoff et al., 2015b). The magnitude of heat wave impacts may be changing related to the vulnerable sectors affected, particularly to those exposed through poor health and low and high age (Basu and Samet, 2006). The rapid increase of the population and urbanization in Georgia and its strong dependence on agricultural production might amplify these negative heat health impacts (UNDP, 2015). Yet, heat health is an under-reported sector in Georgia with economic consequences that are currently difficult to assess.

Excess mortality has been observed during several heat wave events over the last five decades (Semenza et al., 1996; Changnon et al., 1996; Nairn, 2011; Nairn and Fawcett, 2013; Langlois, 2013). In the present study the heat wave index based on the Excess Heat Factor is used to investigate heat wave changes during the last 50

ESDD
6, 2273–2322, 2015

to 30 years and to identify high-impact heat waves over Georgia and their patterns using daily composites. The EHF considers the local geographic acclimatization to temperature, the total heat load, and the recent deviation in temperature from mean temperature (Nairn, 2011; Nairn and Fawcett, 2013; Nairn et al., 2015). Next to maximum temperature, the increase in morbidity and mortality is sensitive to high minimum temperatures. Minimum temperature, which is dissipated precedent to a very hot day, determines the accumulating daytime thermal load impacting vulnerable people and systems (Pattenden et al., 2003; Nicholls et al., 2008). In general, the health effect may be induced by both, a combination of high intensity maximum and minimum temperature and long heat wave duration (Nairn et al., 2015).

The frequency, duration and intensity of heat wave events is usually linked to large-scale atmospheric blocking patterns enhancing Sea Surface Temperature, solar radiation and heat flux anomalies due to reduced cloudiness and/or antecedent precipitation and soil moisture deficiencies. The core mechanisms for heat accumulation are (1) advection from lower latitudes, (2) large-scale subsidence transporting higher potential temperature air from upper levels, or (3) surface heating, development of the diurnal mixed layer, and replacement from below by the new mixed layer for the successive day (McBride et al., 2009). A growing number of studies have investigated the mechanisms that contribute to the formation and prediction of heat wave events using the example of high-impact events in Eurasia, such as the 2003 European heat wave (Black et al., 2004; Fink et al., 2004; Ogi et al., 2005; Trigo et al., 2005; Ferranti and Viterbo, 2006; Jung et al., 2006; Fischer et al., 2007; Black and Sutton, 2007; Feudale and Shukla, 2011a, b), or the 2010 Russian heat wave (Barripedro et al., 2011; Dole et al., 2011; Grumm, 2011). Most studies relate heat wave events to anticyclonic circulation anomalies, leading to enhanced heat advection, adiabatic heating by subsidence and solar radiative heating due to reduced cloudiness (Black et al., 2004; Meehl and Tebaldi, 2004; Fink et al., 2004; Della-Marta et al., 2007; McBride et al., 2009; Cassou et al., 2005; Carril et al., 2008; Stefanon et al., 2012; Pfahl and Wernli, 2012; Zittis et al., 2014). Next to synoptic features Sea Surface Temperature (SST) anoma-

ESDD
6, 2273–2322, 2015

lies (Jung et al., 2006; Black and Sutton, 2007; Della-Marta et al., 2007; Feudale and Shukla, 2011a, b), precipitation and soil moisture deficiencies can represent crucial driving forces contributing to current and future heat wave events (Ferranti and Viterbo, 2006; Fischer et al., 2007; Zampieri et al., 2009; Seneviratne et al., 2010; Hirschi et al., 2011; Jäger and Seneviratne, 2011; Müller and Seneviratne, 2012; Quesada et al., 2012; Stefanon et al., 2014; Zittis et al., 2014).

Current scientific literature investigated relationships between heat wave events and their mechanisms of formation and prediction, using the example of selected patterns or in the context of single heat wave events. Moreover, most papers focus on large study areas, excluding regional aspects of relationships between heat waves and their driving forces. Due to the fact that observation data for Georgia is difficult to access and the country is located at in a transition zone between Europe and Asia and common study areas, such as the Mediterranean and the Eastern Mediterranean and Middle East (EMME) Region, Georgia is often marginalized in study domains. The aim of this study is to quantify summer heat wave changes and variability over Georgia and to provide a comprehensive understanding of their forcing mechanisms. In Sect. 2 data and methods utilized are presented. Section 3.1 demonstrates major severe summer heat wave identification. Section 3.2 presents the climatology and trends in the summer heat wave number intensity, duration and their potential forcing predictors during the analysis periods 1981 to 2010 and 1961 to 2010. In Sect. 3.3 results on heat wave patterns from daily composites and a CCA are discussed. Section 4 summarizes results and the conclusions of the study.

2 Data and methods

2.1 Observation data

For the heat wave trend and identification analysis 22 daily minimum and maximum temperature series covering the period 1961 to 2010 have been used (Fig. 2). Data

ESDD
6, 2273–2322, 2015

and Metadata for homogenization adjustment was kindly provided by the National Environmental Agency of Georgia. The analysis period 1961–2010 was chosen to study changes in heat wave characteristics under anthropogenic influenced climate conditions as well as to optimize the number of stations available and spatial coverage. The stations are well distributed over Georgia. During 1988, 1992 and 1993 data availability for observation data records was very low and had to be rejected from the analysis. Data quality control has been carried out using the computer program RClimDex Software version 1.1 available on http://etccdi.pacificclimate.org. During the index calculation process the following data quality requirements have been applied in order to include as many Georgian temperature series as possible: (1) a summer value is calculated if all months are present (May to September), (2) a month is considered as complete if ≤ 3 days are missing, (3) a station will be rejected from the analysis if more than 5 consecutive months are missing. In order to test data homogeneity and to adjust significant breakpoint, the software package RHtestV3 was used. It has been developed in order to detect and adjust multiple breakpoints in a data series with noise that may or may not have first order autocorrelation (Wang and Feng, 2010; Wang, 2015). Details on quality control, homogeneity testing and adjustment procedure and parameter usage during the QM adjustment procedure are stated in Keggenhoff et al. (2015a).

2.2 Reanalysis data

Reanalysis data is used to detect spatial and temporal absolute differences and trends and to examine the dynamical evolution and features associated with heat waves over Georgia and Eurasia. Data was provided by the National Centers for Environmental Predictions-National Center for Atmospheric Research (NCEP-NCAR) and Kalnay et al. (1996). For Sea Surface Temperature (SST) the Reynolds Optimum Interpolation (OI) Analysis V2 data-set is used (Reynolds et al., 2002). The NCEP-NCAR records are archived in grids of a resolution $1.88^{\circ} \times 1.88^{\circ}$, the spatial resolution of the SST reanalysis data measures $1.00^{\circ} \times 1.00^{\circ}$. The reliability of the NCAP/NCAR temperature data was verified correlating the reanalysis data with the observed data (Pearson

ESDD
6, 2273–2322, 2015

correlation). Between 1961 and 2010 the mean summer temperature for the field 39.9–46.9° E/40.9–43.7° N correlates very well with the mean temperature (r^2: 0.76) from the observational data. For Tmax and Tmin the correlation coefficient measures 0.67 and 0.77, respectively.

2.3 Heat wave identification and severity classification

For generating daily composites for major extreme heat wave days this study uses the heat wave index based on the EHF as defined by Nairn (2011). The EHF was calculated using the *Clim*PACT software, a R-based software. It includes both, daily maximum and minimum temperature series and incorporates the effect of humidity on heat tolerance indirectly, by using the mean, rather than the maximum daily temperature, in the calculation. EHF values are calculated from a three-day mean of forecast temperatures to derive an index of heat wave severity. Two sub-indices are combined to produce the complete EHF index. The first is a measure of significant excess heat relative to local climatic conditions, the 95th percentile of mean temperature conditions:

$$\mathrm{EHI}_{\mathrm{sig}} = (T_i + T_{i+1} + T_{i+2})/3 - T_{95}. \quad (1)$$

The second sub-index is a measure of shorter term acclimatization to heat, relative to the mean temperature of the previous 30 days:

$$\mathrm{EHI}_{\mathrm{accl}} = (T_i + T_{i+1} + T_{i+2})/3 - (T_{i-1} + \ldots + T_{i-30})/30. \quad (2)$$

These two indices are combined to generate the EHF index. The unit of EHF is °C^2:

$$\mathrm{EHF} = \mathrm{EHI}_{\mathrm{sig}} \times \max(1, \mathrm{EHI}_{\mathrm{accl}}). \quad (3)$$

The EHF provides a comparative measure of intensity, load, duration and spatial distribution of a heatwave event and has a strong signal-to-noise ratio. According to Collins et al. (2000) and Pezza et al. (2012) the definition of the heat wave index comprises

ESDD
6, 2273–2322, 2015

three or more consecutive days above positive EHF conditions. The magnitude of heat health impacts caused by heat waves is indicated foremost by the peak heat load ($°C^2$) of a heat wave (Nairn and Fawcett, 2013). To distinguish between EHF days, severe and extreme heat wave days during 1961 and 2010 the severe EHF threshold for each station has been included in the analysis, which is calculated according to Nairn and Fawcett (2013). Severe heat waves are defined by an event where EHF values exceed a threshold for severity that is specific to the climatology of each location. The severe EHF threshold is calculated empirically as the 85th percentile of the distribution of positive EHF values (EHF85) based on the observation record at a given location. This method ensures that all EHF values are truly representative of each site's climatology and avoids potential errors by modelling a distribution. Extreme Heatwaves are defined as an event where EHF values are well in excess of the severity threshold and result in a wide impact based on a cascade of failing systems. According to Nairn et al. (2015), extreme heat waves are detected if an EHF value during a heat wave at least triples the station's severity threshold (EHF $\geq 3 \times$ EHF85). The resulting heat wave aspects: HWday – the number of heat wave days (days with positive EHF value), HWsev – the number of severe heat wave days and HWext – extreme heat wave days enable to differentiate between heat waves with low to high heat health impacts based on their exceedance of a station's severe EHF threshold. The heat wave aspects are calculated annually over a 5 month summer, which is defined as a period from May to September (153 days). In order to identify the major single heat wave days for the daily composite analysis extreme EHF values are classified as heat wave classes (HW class), depending on the difference between an EHF value and the respective station's severe threshold. In the present study all extreme EHF values could be classified into five different classes (HW class 2 to 6) with a maximum heat wave class of six. The 16 major heat wave days between 1961 and 2010 over Georgia were detected selecting all heat wave days equal or above heat wave class 4 (EHF $\geq 4 \times$ EHF85). All identified heat wave days are listed in the Annex.

ESDD
6, 2273–2322, 2015

Mean absolute differences (subtracting the period 1961–1990 from 1981–2010) and trends between the periods 1961–2010 and 1981–2010 have been detected for observed heat wave events and the selected predictand and predictor variables. Observed heat wave events have been calculated for four heat wave aspects: HWN – the yearly number of heat waves, HWD – the length (in days) of the longest yearly event, HWF – the sum of participating heat wave days per year, and HWext – extreme heat wave days. Throughout the analysis, monthly mean data for summer months (May to September) are used. All trends were calculated by the non-parametric Sen's slope estimator based on Kendall's tau (τ) (Sen, 1986). Observed trends are calculated as the arithmetic average of the summer index values of stations with more less than 20 % missing data. The annual slopes of trends were converted into slope per decade. The statistical significance has been estimated using the Mann–Kendall test and the statistical significance level of the 5 % has been used (Mann, 1945; Kendall, 1975). In this study any use of the word "significant" implies statistical significance at the 5 % level.

2.4 CCA and composite analysis

The statistical relationship between predictor and predictand variables ususally is a linear regression relationship. In order to investigate the relationship between Georgian summer heat waves and synoptic to meso-scale patterns over Eurasia, a CCA was performed. CCA is a common multivariate statistical technique in meteorological and climate science to find linear combinations of two sets of variables such that the linear combinations have the maximum possible correlation (Barnett and Preisendorfer, 1987; Bretherton et al., 1992; Cherry, 1996). The maximization is carried out under orthogonality constraints on the coefficients of the linear combinations. CCA has been used in various studies (e.g. Xoplaki et al., 2003a, b, Haylock and Goodess, 2004; Luterbacher et al., 2009). During data preparation monthly mean anomalies are calculated by subtracting the long-term mean of a calendar month from each individual monthly mean, giving all grid points equal weight. Moreover, a long-term linear trend in the time series is removed. Using Principal Component Analysis (PCA) the predictor and predictand

ESDD
6, 2273–2322, 2015

were dimensionally reduced to a number of selected Principal Components (PCs) in order to identify the dominant patterns of variability in each field that account for the most variance (Bretherton et al., 1992; Mo and Straus, 2002). Both, the CCA and PCA were performed using a Singular Value Decomposition (SVD) using the KNMI Climate Explorer (http://climexp.knmi.nl). The correlation of the canonical score series of the two variables measures the intensity in the relationship between the pairs. In this study, the 95th percentile of mean temperature (Tmean95p) is used as heat wave predictand derived from daily NCEP/NCAR reanalysis data. It includes both, daily minimum and maximum temperature series and incorporates the effect of humidity on heat tolerance indirectly, by using the mean, rather than the maximum daily temperature, in the calculation. The 95th percentile threshold was chosen as a measure of extreme heat. Data availability ensures a high number of heat days per summer month. As predictors summer SLP, Z500, u-wind500, v-wind500, O500, RH500, OLR, RR and SM were used based on gridded NCEP-NCAR data have been used. The research domain for the predictors is defined as the area between 0 and 90° E and between 10 and 80° N. The predictand variable focuses on Georgia with the domain located at 39.9 to 46.9° E and 40.9 to 43.7° N. Features in the daily composite anomaly plots take into account the physical realism as they are based on observation data, whereas the derived CCAs are statistically built. To examine the observed features associated with the CCA patterns, daily composite plots are conducted, since the CCA may yield unstable solutions (Della-Marta et al., 2007). Daily composites are constructed for the heat wave predictand and the ten selected predictors based on the 16 major heat wave days observed over Georgia listed in the Annex.

ESDD
6, 2273–2322, 2015

3 Results and discussion

3.1 Heat wave identification

A heat wave is defined as a period of three or more consecutive days above EHF conditions. All station heat waves during 1961 and 2010 have been identified and their duration (days), heat load ($^{\circ}C^2$) and accumulated heat load ($^{\circ}C^2$) have been determined. According to Nairn and Fawcett (2013) the heat load of a heat wave is defined as the mean all EHF values of a heat wave. The accumulated heat load represents the sum of all EHF values of a heat wave. In the present study most severe heat waves have been ranked by their Georgia-average accumulated heat load considering the average duration of a heat wave and its heat load as their product. Table 1 lists the 10 summers with the most severe heat wave events over Georgia since 1961. It describes the rank, the date of the peak EHF (Date), the duration (days), intensity ($^{\circ}C^2$) and the accumulated heat load ($^{\circ}C^2$) averaged over the all stations analyzed, respectively. Heat waves with a mean accumulated heat load of less than 15 $^{\circ}C^2$ were not listed.

As shown in Table 1 only two heat waves (June 1966 and 1969), which are among the ten most severe heat waves, occurred before 1990. Major heat waves observed after 1990 comprise the highest ranked accumulated heat loads, heat loads, lengths and number of occurrence. The three most severe heat waves identified occurred in May 2007, in August 2006 and in June 1998 and agree with the most fatally heat waves reported by EM-DAT for the region (The International Disaster Database, www.em-dat.be). The highest Georgia-averaged accumulated heat load (200 $^{\circ}C^2$) was observed for the severe heat wave in May 2007. The mean heat load of this event was the highest measured during 1961and 2010 (20.0 $^{\circ}C^2$), although the mean duration for this heat wave is mid-ranged (10 days), implying strong health impacts by a high intensity of heat load. All stations analyzed have been affected by this event and at the same time show extraordinary high peak EHF values of up to 57.5 $^{\circ}C^2$ (HW class 6). The second ranked heat wave was observed during mid-August. It shows an extraordinary long averaged duration of 18 days, resulting in a mean accumulated heat load

ESDD
6, 2273–2322, 2015

of 127 °C^2. At the same time the mean heat load (7.1 °C^2) is relatively mid-ranked. The heat wave is closely followed by another severe heat wave, which is ranked 7, implying strong heat impacts caused by the long averaged duration of both events and their close occurrence. For the third most severe heat wave identified (June 1998) a mean accumulated heat load of 114 °C^2 was determined. Both, the event's averaged duration (14 days) and the averaged heat load (8.4 °C^2) are clearly above average values and the proportion of affected stations is very high, which results in a high averaged accumulated heat load. This heat wave was observed among four other summer heat waves in 1998, which is – next to 2010 – a year with the highest count of summer heat waves measured.

3.2 Climatology and heat wave changes

3.2.1 Observed long-term trends

In this section the climatology and recent changes in observed summer heat waves during the periods 1961 and 2010 and 1981 and 2010 are investigated. As shown in Table 2, the absolute Georgia-average for HWN (the number of heat wave events) amounts to 1.7 events yr^{-1} and shows a significant increasing trend of 0.4 events decade^{-1}. HWD (the length of the longest yearly heat wave event) measures 5.5 days yr^{-1} in the Georgia-average and a significant positive trend of 0.9 days decade^{-1} is found. The Georgia-average for HWF (yearly sum of participating heat wave days) measures 10.4 days year^{-1}. Similar to HWN and HWD, no decreasing station trend could be observed throughout Georgia (not shown). The Georgia average trend amounts to 2.9 days decade^{-1} (Table 2). These findings are in accordance with Perkins et al. (2012) and Perkins and Alexander (2013), demonstrating that the high trend magnitudes for HWF drive increases in HWN and HWD, as the number of heat wave days represents an influencing factor in the calculation of event length and occurrence. For HWex (extreme heat wave days) an absolute mean of 0.3 days and a significantly increasing trend of 0.05 days decade^{-1} are observed.

ESDD
6, 2273–2322, 2015

As Fig. 3 shows all mean absolute differences for the heat wave occurrence, intensity and duration were found to be positive. For HWN an absolute increase between 0 and 1 event can be observed during the period 1981 and 2010 (with respect to the period 1961–1990). A few stations in the south and northwest of Georgia show an increase of 1 to 2 events. HWD shows an increase between 0 and 3 days for the major proportion of stations analyzed. For 5 of 22 stations the duration of heat waves increased to 3 to 6 days between 1981 and 2010. The heat wave aspect HWF shows an increase of 8 to 16 days for 6 of 22 stations analyzed during 1981 and 2010. For HWex an increase between 0 and 2 days can be found for the highest proportion of stations. For seven stations a strong increase by 3 to 6 extreme heat wave days is found.

Comparing the trends in the heat wave aspects HWN, HWD, HWF and HWex over Georgia for the two analysis periods 1961–2010 and 1981–2010, a pronounced increase in the magnitude of all trends is observable. Significant trends are found for HWN, HWD and HWF. As Table 2 shows trends for HWN and HWD (1981–2010) double the trend magnitudes measured for the period 1961–2010. A trend of 0.8 events decade^{-1} for HWN and 1.8 days decade^{-1} for HWD could be found. For HWF (and HWex), the trend magnitudes of 6.6 days decade^{-1} (0.15 days decade^{-1}) for 1981 and 2010 are even two to three times higher the trend magnitudes observed between 1961 and 2010.

3.2.2 Trends in the heat wave predictand and predictors

In this section the climatology and spatio-temporal changes of the heat wave predictand and selected predictors for the analysis periods 1961 to 2010 and 1981 to 2010 are presented.

As Table 3 shows, the climatological mean for Tmean95p averaged over Georgia was measured 20.4 °C. The absolute increase comparing the periods 1961–1990 and 1981–2010 amounts to 0.1 °C. Trends for the heat wave predictand Tmean95p were observed to be positive. During the analysis period 1961–2010 an insignificant warming trend of 0.2 °C decade^{-1} (significant at the 10 % level) could be found over Georgia.

ESDD
6, 2273–2322, 2015

A significant trend for Tmean95p was observed between 1981 and 2010, which measures 0.4 °C decade^{-1}. As shown in Fig. 4a spatial changes in Tmean95p, large areas with an absolute temperature difference of more than 0.6 °C from Eastern Europe to the Ural Mountains are detected with peaks of up to 1 °C, although no significant difference could be found. Also for Turkey and eastern Georgia an insignificant increase of 0.2 to 0.6 °C could be observed. However, in western Georgia an insignificant increase in Tmean95p of at most 0.2 °C was found.

As presented in Table 3, the Caspian Sea shows a higher climatological mean for SST (21.6 °C) than the Black Sea (20.2 °C). For the Caspian Sea a significant SST trend magnitude of 0.7 °C decade^{-1} during the period 1981 to 2010 could be observed, while for the Black Sea a significant magnitude of 0.6 °C decade^{-1} was found. The spatial distribution of SST absolute differences shows significant warming in the North Atlantic, The Mediterranean, Black and Caspian Sea (Fig. 4b). Largest differences of significant warming over Eurasia are found in the North and Baltic Sea and in the Kara Sea (0.6–0.8 °C).

As shown in Table 3 the climatology for SLP measures 1012 mb with an absolute increase throughout Georgia of 1.2 mb. While a significant trend magnitude for the period 1961–2010 of 0.5 mb decade^{-1} could be observed, no change between 1981 and 2010 was detected. Figure 4c shows large areas of significant positive trends in the eastern Mediterranean, Western Asia and Northern Africa. A maximum of significant absolute change in SLP is found in northeast Turkey and stretching throughout Georgia measuring an increase of up to 2 mb.

For Z500 a mean climatology of 5753 m was detected over Georgia and an absolute increase of 15.9 m with respect to the period 1961–1990 (Table 3). A significant positive trend for Z500 of 8.7 m decade^{-1} could be found during the period 1961 and 2010. However, the trend magnitude for the period 1981–2010 was smaller (2.3 m decade^{-1}) and insignificant. As shown in Fig. 4d, throughout southern Eurasia a significant absolute increase of Z500 of up to 20 m is observed, which corresponds to observations for Western Asia by Kuglitsch et al. (2010). These findings highlight a changing atmo-

ESDD
6, 2273–2322, 2015

spheric circulation over Georgia, implying an increase in warm air advection from the Southwest, large-scale subsidence and surface heating, which might have enhanced the formation and persistence of heat waves in recent years. Moreover, the increase in Z500 is usually connected with the increase in stability and the inhibition of convection over the area.

For u-wind an absolute decrease of $0.6\,m\,s^{-1}$ is observed comparing the periods 1961–1990 and 1981–2010. Georgia-averaged climatological mean measures $6.8\,m\,s^{-1}$ (Table 3). Trends for the zonal wind are insignificant during both analyzing periods. The climatology for v-winds measures $3.7\,m\,s^{-1}$ with an absolute decrease throughout Georgia of $-0.5\,m\,s^{-1}$. While a significant trend magnitude for the period 1961–2010 of $-0.2\,m\,s^{-1}\,decade^{-1}$ could be observed, an insignificant change of $0.0\,m\,s^{-1}\,decade^{-1}$ between 1981 and 2010 was detected.

As shown in Fig. 5a OLR measures a mean climatological value of $246\,W\,m^{-2}$ and an absolute increase of $5.8\,W\,m^{-2}$, implying a decrease in cloudiness and an increase in maximum insolation. During the period 1961–2010 a significant positive trend of $2.9\,W\,m^{-2}\,decade^{-1}$ could be observed. As all other predictors OLR shows an increase in the trend rate during 1981 and 2010 compared to the period 1961–2010 ($3.1\,W\,m^{-2}\,decade^{-1}$) (Table 3). The spatial distribution of OLR trends shows an increase throughout Western Asia with the highest absolute increase of up to $12\,W\,m^{-2}$ located across the Caspian Sea (including Eastern Georgia). Vertical Velocity at 500 mb measures an absolute increase of $0.01\,Pa\,s^{-1}$ comparing the periods 1961–1990 and 1981–2010 averaged over Georgia. The trend magnitude during the period 1961 to 2010 measures a significant increase of $0.01\,Pa\,decade^{-1}$ over Georgia. The trend for the period 1981–2010 shows a higher magnitude of $0.02\,Pa\,decade^{-1}$, but is insignificant. Regarding the spatial distribution of absolute changes during 1961 and 2010 a significant positive difference of up to $0.015\,Pa\,s^{-1}$ is located in Azerbaijan and northern Iran (Fig. 5b), suggesting an increase in atmospheric stability and subsidence. However, negative but mainly insignificant areas are located across the eastern Mediterranean and Black Sea as well as in the east of the Red and Caspian

ESDD
6, 2273–2322, 2015

Sea and the Persian Gulf, implying an increase in instability and convergence. The location of these areas resembles the centers of zero trends in the OLR trend map (Fig. 5a), supporting the implication of local decreases in clear skies and insolation. Georgia shows a maximum absolute change of around 0.01 $Pa\,s^{-1}$ in the eastern part decreasing towards the western coast until approximately zero. As presented in Table 3 for RH500 a climatological value of 44 % could be observed. An absolute decrease of −4.8 % was found and a significant trend of −2.4 % $decade^{-1}$ was measured during 1961 and 2010. The spatial distribution of absolute changes shows similar patterns. RH500 shows significant decreases of up to −0.06 % across the Caspian Sea (Fig. 5c) with lowest values in the eastern part of Georgia and higher insignificant differences of around −0.04 % to the West of Georgia. The reduction of air humidity is also found by Kuglitsch et al. (2010) detecting decreasing RH500 over West Asia accompanied by an increase in minimum and maximum temperature, Z500 and SLP.

For RR an absolute decrease of −0.7 $mm\,day^{-1}$ observed comparing the periods 1961–1990 and 1981–2010. Georgia-averaged climatological mean for RR measures 5 $mm\,day^{-1}$ (Table 3). Trends for RR are significantly decreasing by −0.35 $mm\,day^{-1}\,decade^{-1}$ regarding the period 1961 and 2010. The negative trend magnitude of −0.58 $mm\,day^{-1}\,decade^{-1}$ for the period 1981 to 2010 was even larger, but insignificant (Table 3). As implied by Fig. 5d, absolute differences in the spatial distribution of total precipitation shows a large area of significant decreasing rates by −1.2 $mm\,day^{-1}$ predominantly in the east of Turkey, southern Georgia, Armenia, Azerbaijan and northern Iran. Similar to the RR, SM shows decreasing trends over the last five decades. As Table 3 shows, the climatological mean averaged over Georgia was measured 0.3 % and the absolute decrease amounts to −0.01 % comparing the periods 1961–1990 and 1981–2010. Trends for the heat wave predictor SM were found to be negative. During the analysis period 1961–2010 a significant decreasing trend of −0.004 % $decade^{-1}$ could be found over Georgia. However, the trend magnitude for the period 1981–2010 was even larger (−0.007 % $decade^{-1}$), but insignificant. Regarding the spatial distribution of SM change, significant decreasing rates are found in central

ESDD
6, 2273–2322, 2015

and eastern Turkey, northern Iran and the Southern Caucasus. Towards northwestern Georgia the trend measures approximately zero. The spatial location of high reduction rates of RR, SM and RH500 have a strong resemblance of those measuring a high increase in SLP, Z500, OLR and O500, which supports the assumption, that the increase in surface heating, subsidence and warm air advection drive the reduction in air humidity, total precipitation and soil moisture.

3.3 Heat wave related weather patterns

In order to examine the related features associated with the 16 major summer heat wave days over Georgia, daily composites of ten large- to meso-scale surface and mid- troposphere fields over Eurasia are presented. All anomalies were calculated with respect to the period 1981 to 2010. Moreover, the coupled variability of the selected predictors and the heat wave predictand (Tmean95p) is investigated by performing a CCA. All CCA patterns show a close resemblance to the daily heat wave composites. Because the higher CCA modes explain negligible amounts of variance, this paper focuses only on the analyses of the first CCA mode for each predictor, respectively. For the sake of brevity, CCAs for the heat wave predictand over Georgia are not shown. Table 4 shows the results of the CCA listing the potential heat wave drivers, their domain, the temporal correlation coefficients of the score series between each predictor and local extreme temperature and their explained variance with the respective 95 % confidence interval to validate the model skill across the domain. As shown in Table 4, all confidence intervals suggest a good to very good skill over the entire domain, except for the SST and SLP domains for Eurasia and the Black Sea, which are rather good to poor.

3.3.1 Temperature and SST patterns

As shown in Fig. 6a, western and central Europe and western Asia are dominated by negative SAT fields, associated with the surface cyclones over the area. However,

ESDD
6, 2273–2322, 2015

Eastern Europe, the Mediterranean and Middle East as well as from Northern Africa to Western Russia warm centers are observed during major heat wave events over Georgia. Two centers of high SAT anomalies of up to 5 °C were found in Armenia and in the southern Ural Mountains. The SAT anomaly over Georgia stretches from 2.5 °C in the Northwest up to 5 °C in the Southeast, implying strongest heat-health impacts here. The centers of negative SAT anomalies with a maximum of −3 °C lie southeasterly and southwesterly of the positive heat anomalies below the middle level cyclones (see Fig. 7b).

SST anomalies suggest a close relationship between large-scale dynamic patterns as shown in Fig. 6b. While the Northern Atlantic and Eastern Mediterranean Sea show negative SST anomalies of up to −0.6 °C, positive SST anomalies are observed in the Caspian Sea of up to 0.7 °C. Lower positive SST anomalies can be found in the Eastern Black Sea (0.5 °C). Highest anomalies are found in the Barents and Kara Sea of up to 1 °C during heat wave events over Georgia. The SST pattern for the first CCA mode over Eurasia demonstrates a very close resemblance to the SST composite for observed heat wave events and accounts for approximately 52.3 % of the summer heat wave variability over Georgia (Figs. 6b and 9g). The squared correlation between the summer SST and heat wave pattern is 0.56. Although a close relationship between SSTs and heat waves could be observed, it does not necessarily mean that the SST anomalies are responsible for heat waves over Georgia. It is far more likely that SST anomalies are an accompanied phenomenon of extreme temperature events. Nevertheless, the possibility that an individual heat wave might be affected by local SST anomalies cannot be excluded. Composite and CCA fields have a strong resemblance with the SAT and Z500 fields suggesting enhanced local air advection, subsidence and maximum insolation over strong SST warming fields during heat wave events, which is in accordance with Feudale and Shukla (2011a). Moreover, the reduction of meridional winds over sea, mainly apparent over the southern Caspian Sea, prevents the generation of lee waves and cyclones (Fig. 7d). Hence, the cooling effect by wind-induced mixing is reduced, which further warms up the SST (Buzzi and Tibaldi, 1978). The si-

ESDD
6, 2273–2322, 2015

multaneous SST anomalies in the Caspian, Northern Barents and Kara Sea can be explained by a reduction of baroclinic instability between the Southern Caucasus and the Northern Barents and Kara Sea, as discussed by Feudale and Shukla (2011a) for the simultaneous SST anomalies in the Mediterranean and the Northern Atlantic during the heat wave 2003. The prevention of baroclinicity is caused by a diminishing land–sea temperature gradient, which is reflected by the negative anomalies of v-winds over the Northern Barents Sea and West Asia stretching from Northeastern Africa across the Southern Caspian Sea to the Kara Sea (Fig. 7d) resulting in a northward shift and intensification of the subtropical jet and a northward shift of the African ITCZ.

3.3.2 Large-scale circulation and mid-troposphere patterns

As shown in Fig. 7a, a deep surface trough is found over Southern Scandinavia extending across the Black Sea area towards the Persian Gulf and the Red Sea. The persistent surface lows are known as the "Persian Gulf trough" and "the Red Sea trough", which govern a strong relation to heat waves and heavy precipitation in the Mediterranean (e.g. Ziv et al., 2004; de Vries et al., 2013). At the same time, pronounced anticyclones are located over the Ural Mountains, the Mediterranean Sea, North Africa and Iran, implying warm air attraction from the Mediterranean and Middle East to Georgia (Fig. 7a). The SLP composite and CCA mode over Eurasia show similar patterns during heat wave events (Figs. 7a and 9a). The first CCA mode captures 61.2 % of the summer heat wave variability. The squared correlation between the summer SLP and heat wave predictand amounts to 0.62. The observed heat wave patterns have a strong resemblance to those found for heat waves in Western Asia by Kuglitsch et al. (2010).

Composite and CCA patterns for Z500 demonstrate a large anticyclonic vortex with anomaly maxima of 90 m during major heat wave events. Negative anomalies of up to −60 m are located westerly over the British Isles, Southern Scandinavia and easterly over central Asia and central Russia. Over eastern Georgia positive anomalies of around 60 m are found, while towards the western coast the intensity decreases to 40 m. The first CCA mode shows a close resemblance to the composite and captures

ESDD
6, 2273–2322, 2015

61.6 % of the summer heat wave variability (Figs. 7b and 9b). The squared correlation between the summer Z500 and the heat wave predictand measures to 0.74. The location of the middle tropospheric troughs over Scandinavia and West Asia are in southeasterly and southwesterly location aside of the anticyclonic center resembling a typical west-oriented omega high, a nearly-stationary anticyclonic pressure field closely associated to high-impact heat waves (Fig. 7b). The observed pattern can be referred to the "RU (Russian) cluster" identified as one of six heat wave blocking patterns identified by Stefanon et al. (2012) or to the "Eurasia" region, one of three regions, in which the frequency of the extremely hot days per month homogeneously varies (Carril et al., 2008). Due to its location it is known as the Ural Blocking High (UBH) pattern and is associated with the 2010 Russian heatwave investigated by Barriopedro et al. (2011), Dole et al. (2011) and Grumm (2011). The blocking of westerlies is caused by a reduction of baroclinicity, which is typical for the mid-latitudes. In general, baroclinic instability enhances the blocking persistence, the interruption of the mid-latitude westerlies, the deflection of the west–east storm tracks, large-scale subsidence and incoming solar radiation. Baroclinicity usually limits the northern branch of the Hadley cell expanding to the North. Reduced baroclinic activity during heat waves leads to a northward shift of the descending branch of the Hadley cell and the African ITCZ, which is consistent with studies on heat waves over Eurasia by Cassou et al. (2005) and Carril et al. (2008). As shown in Fig. 8b, the precipitation composite over the central Sahel implies a northerly shift of the African ITCZ. This relation was first investigated by Rowell (2003), which observed an increase of rainfall over the western African Sahel and a northern shift of the African ITCZ during warm Mediterranean SST.

The u-wind composite and CCA mode is consistent with reduced baroclinicity and shows reduced zonal wind activity throughout central Asia of up to $-9\,\mathrm{m\,s^{-1}}$. An enhanced zonal wind flow is deflected by the anticyclonic center, implying a northward shift of the subtropical jet. Regarding Georgia, reduced wind speeds of $-4\,\mathrm{m\,s^{-1}}$ are found in the eastern part and increase towards $1\,\mathrm{m\,s^{-1}}$ in the West, implying stronger influence of the anticyclonic blocking and associated subsidence in the Western part

ESDD
6, 2273–2322, 2015

of Georgia (Fig. 7c). V-winds at 500 mb intensify over Western Russia by up to 9 $m s^{-1}$, proving warm and dry air masses are attracted from south-southwest during major heat wave events. Negative anomalies are found from Northeastern Africa across the Southern Caspian Sea to the Kara Sea, implying a reduced meridional gradient between continental central Asia and the Northern Barents and Kara Sea (Fig. 7d). In western Georgia positive anomalies of over 7 $m s^{-1}$ can be observed, while anomalies in the southeast of approximately zero can be found, implying a stronger relation of warm air advection and heat wave events are found in the West. The u- and v-wind composites and CCA modes show a strong resemblance (Figs. 7c, d and 8c, d). The squared correlation between the summer zonal wind and the heat wave predictand amounts to −0.77. The first CCA mode for u-wind captures 59.4 %, whereas the CCA pattern for v-wind accounts for 62.4 % of the summer heat wave variability (Fig. 9c and d). The squared correlation between the summer meridional wind and the heat wave predictand measures 0.76.

The analysis of vertical pressure velocity at 500 hPa reveals two opposing patterns affecting Eastern and Western Georgia differently (Figs. 7e and 9e). The first O500 CCA mode captures 55.5 % of the summer heat wave variability. The correlation between the summer O500 pattern and the heat wave predictand amounts to 0.81, implying a strong relation between subsidence patterns and the heat wave occurrence in Eastern Georgia. Similar to the CCA pattern, the composite detects intensified O500 of up to 0.7 $Pa s^{-1}$ located over the Caspian Sea and central Asia associated with local stability, subsidence, clear skies and maximum insolation during major heat wave events. Throughout Western Russia and the Barents Sea positive, but weaker anomalies are observed. These patterns mainly influence heat wave patterns over eastern Georgia, whereas a band of negative O500 anomalies (correlation fields) is found across the eastern Black Sea and West Georgia. Reduced vertical pressure velocity over Southern Scandinavia and central Asia as well as those stretching from northeast Africa to southwestern Russia are characterized by instability, convection and cloudiness, reflected by the decrease in enhanced surface heating and precipitation

ESDD
6, 2273–2322, 2015

(Fig. 8a and c). High SATs combined with high SSTs lead to increased latent heat fluxes (Xoplaki et al., 2003a) and increased air humidity, hence convection and precipitation.

As presented in Fig. 7f, composite anomalies for relative humidity at 500 mb during major heat wave events show lowest values of up to −20 % over central Asia, eastern and southeastern of the Caspian Sea. Negative fields are also found northeastern of the Black Sea, over central Russia and the Barents and Kara Sea. The observed heat wave patterns have a strong resemblance to climate composites of major heat wave events in the eastern Mediterranean found by Kuglitsch et al. (2010). They also show a close relation to SLP, O500 and OLR patterns (Figs. 7a, e and 8a). Because of the atmospheric stability, vertical motion is restricted to the lower boundary layer, where solar radiation is maximized and the warm air is trapped. The spatial distribution of RH500 CCA fields shows similar patterns (Fig. 9f). The first CCA for RH500 mode captures 52.1 % of the summer heat wave variability. The squared correlation between the summer fields for RH500 and the heat wave predictand over Georgia amounts to 0.78.

Figure 7g shows a vector wind composite during heat wave events and provides evidence, that anomalously strong, warm and dry winds collect moist over the warm eastern Mediterranean and Black Sea producing cyclones and strong convective rainfall events above western Georgia (Fig. 8c). While western Georgia is dominated by moist air masses, eastern Georgia is influenced by warm and rather dry winds from North Africa and the Middle East of much lower wind speed anomalies. Moreover, the Surami Mountain chain dividing western and eastern Transcaucasia holds moist air masses and leads to adiabatic heating by foehns in on the luv side bringing dry air to the East.

3.3.3 Meso-scale surface patterns

High Outgoing Longwave Radiation rates are usually well correlated with high surface temperature, low soil moisture and water vapor concentration in the planetary boundary

ESDD
6, 2273–2322, 2015

layer (Fischer et al., 2007). Figure 8a shows highest OLR anomalies of up to 28 W m^{-2} east of the Caspian Sea during major heat wave events. The spatial distribution of high OLR anomalies corresponds well with areas of high SLP, Z500 and O500 anomalies (Fig. 7a, b and e) as well as low anomalies of relative humidity and zonal winds at 500 mb (Fig. 7c and f), implying enhanced subsidence, clear skies and maximum radiation leading to surface heating. Over eastern Georgia positive anomalies of 8 W m^{-2} can be observed, while west Georgia shows negative OLR anomalies of −8 W m^{-2}, which suggests enhanced cloudiness and atmospheric instability.

Heat waves are usually connected to adjacent rainfall and soil moisture deficits, which is in agreement with Ferranti and Viterbo (2006), Fischer et al. (2007) and Seneviratne (2010). According to precipitation and soil moisture composites illustrating the 20 days prior to the detected major heat wave days, adjacent soil dryness dominates the whole territory of Georgia (not shown). Precipitation patterns during heat wave events are highly influenced by both, the large-scale circulation and local orographic patterns. Large-scale precipitation composite (correlation) fields over Eurasia correspond well with SLP, Z500 and O500 patterns (Figs. 7a, b, e and 9a, b, e). Local precipitation fields are mainly found over mountainous and coastal areas due to moist air advection, instability and convection. Soil moisture fields resemble well the SAT and RR composite and CCA patterns and show negative composite (correlation) fields over Turkey across the Southern Caucasus to Southern Russia (Figs. 6a, 8c, and 9i). Over eastern Georgia simultaneous negative precipitation (−2 mm) and SM fraction anomalies (−0.04) are observed, which supports the evidence of warm and dry air advection, subsidence and surface heating. At the same time, positive RR anomalies of 0.15 mm and negative SM fraction anomalies of −0.03 are observed over West Georgia. Similar to the composite, the CCA pattern detects reduced precipitation over eastern Georgia. The first precipitation and soil moisture CCA mode captures 51.2 % (50.0 %) of the summer heat wave variability (Fig. 9i and j). The correlation between the summer precipitation (soil moisture) patterns and the heat wave predictand amounts to −0.81 (−0.76), implying a strong relation between precipitation and soil moisture deficits dur-

ESDD
6, 2273–2322, 2015

ing heat wave days over Eastern Georgia. This finding is in accordance with Haarsma et al. (2009), who found that summer SAT warming is enhanced due to soil moisture depletion which limits the cooling of the land surface by evaporation. However, as shown in Figs. 7g, 8e and 9i the anomalous southwesterly subtropical winds bring moist air masses to the high mountain ridges of the Caucasus Mountains in Western Georgia, leading to local precipitation maxima at luv sides due to enhanced orographic convection (Kostianoy and Kosarev, 2008). Moreover, soil dryness during heat wave events in mountainous and coastal areas drive instability and air humidity due to meso-scale circulations leading to enhanced precipitation and cooling (Stefanon et al., 2013). This effect could amplify precipitation events and further reduce temperature in mountainous and coastal areas during heat wave events over Georgia.

4 Summary and conclusions

This study detected severity and changes of summer heat wave events over Georgia between 1961 and 2010 and their relationships to large- and meso-scale predictors to identify potential driving mechanisms. Based on the Excess Heat Factor the ten summer heat waves with highest heat health impacts over Georgia were identified in 2007, 2006, 1998, 2001 and 1995. Climatology and heat wave changes between 1961 and 2010 were examined in terms of low- and high-impact intensity, frequency and duration. The observation data used was carefully quality controlled. Homogeneity was tested using the software RClimDex 1.1. Metadata could be used to detect breakpoints and to adjust inhomogeneous time-series using RHVtest 4 (Keggenhoff et al., 2015b).

Summer heat wave changes between the periods 1961–2010 and 1981–2010 revealed significant increasing trends in the Georgia-average. A significant increase for high-impact heat waves (HWex) was measured between 1961 and 2010. HWF shows by far the largest trend magnitudes, which is consistent with findings of Perkins et al. (2012) and Perkins and Alexander (2013), stating that occurrence-based heat wave aspects possess larger trend magnitudes. They also found that the high magni-

ESDD
6, 2273–2322, 2015

tudes of trends for HWF are driving increases in HWN and HWD, due to the fact that the overall number of heat waves (and their duration) will increase when the number of participating days increases. Spatial patterns of trends over Georgia are difficult to assess, which can be attributed to the low data quality and availability. It is also notable that the linear trend magnitude for all heat wave aspects between the analysis period 1981 and 2010 at least double, compared those during 1961 and 2010, implying that more intense and longer heat waves can be expected in future.

The present study focused on a CCA and composite analysis to investigate recent summer heat wave patterns and their relation to the selected atmospheric and thermal predictors over Eurasia: mean Sea Level Pressure, Geopotential Height at 500 mb, Sea Surface Temperature, Zonal and Meridional Wind at 500 mb, Vertical Velocity at 500 mb, Outgoing Longwave Radiation, Relative Humidity at 500 mb, Precipitation and Soil Moisture. Daily composites were conducted for the 16 most intense heat wave days over Georgia between 1961 and 2010. The CCA was performed based on the heat wave predictand Tmean95p over Georgia. CCA is a statistical technique to find spatial patterns of fields with a maximum correlation. The study showed that all composite and CCA patterns have a close resemblance, which verifies both, the composite analysis based on observations and the statistical CCA.

A heat wave study investigating heat wave patterns and predictability over Georgia has been performed for the first time. The results confirmed that large-scale circulation, radiation, precipitation and soil moisture over Eurasia were strongly related to Georgian heat wave events. The analysis detected increasing SAT anomalies over Georgia from West to East. The slight SST anomalies over the Black and Caspian Sea imply no preferred SST pattern inducing heat waves, but that they might reinforce events. The large increase in SSTs in the Barents and Kara Sea during major heat waves over Georgia in combination with a reduction of the meridional gradient and a decrease of baroclinicity amplifies the northward shift of the subtropical jet, allowing the expansion of the blocking high over the Southern Ural. This large anticyclonic pattern is represented by a positive anomaly of Z500 over the area. Moreover, severe heat waves over Georgia

ESDD
6, 2273–2322, 2015

are attributable to negative SLP anomalies over Southern Scandinavia and the Red and Black Sea area and positive SLP anomalies over western Asia. These surface and mid-tropospheric anticyclonic patterns observed (1) block westerlies, (2) attract warm air masses from the Southwest, (3) enhance subsidence and surface heating, (4) shift the African ITCZ northwards, leading to a northward shift of the descending branch of the Hadley cell, and (5) cause a northward shift of the subtropical jet. The regional effects of the persistent blocking are closely related to both, the large- to meso-scale circulation and the local orography of Georgia. The study revealed that Eastern Georgia is mainly influenced by low warm and dry wind flows, subsidence and surface heating due to clear skies, atmospheric stability and maximum insolation, implied by positive anomalies of O500 and OLR and negative RH500, SM and RR patterns over the area. However, during major heat wave events western Georgia is affected by anomalous strengthened wind speed and warm and moist air. These anomalous southwesterly dry winds from Northeast Africa across the Eastern Mediterranean collect moist over the Mediterranean and Black Sea and lead to atmospheric instability and convective rainfall, reflected by negative anomalies for O500 and positive VW500 and RR anomalies over the area. Precipitation might be amplified by the pronounced soil dryness observed throughout Georgia, which induced atmospheric instability and enhanced air humidity and cooling due to meso-scale circulations over mountainous and coastal areas (Stefanon et al., 2013). Moreover, heat waves over Georgia are attributable to reduced soil moisture across the whole territory of Georgia, implying adjacent precipitation deficiency for a prolonged period (Haarsma et al., 2009). This assumption was verified by precipitation and soil moisture composites for a 20 day-period prior to the major summer heat wave events over Georgia. The contribution of lagged precipitation and soil moisture depletion to heat wave events over Georgia will be investigated in more detail in a further study.

Observed changes show that all relevant circulation, radiation and soil moisture patterns contributing to heat waves have been intensified between 1961 and 2010. Tmean95p over Georgia and SSTs over the Black and Caspian Sea showed signifi-

ESDD
6, 2273–2322, 2015

cant warming trends. Largest trends for SSTs are found in the Northern Atlantic and the Kara Sea. Changes in large-scale circulation and radiation patterns reflect a significant increase in surface and mid-troposphere pressure and surface heating throughout Western Asia, while for relative humidity, precipitation and soil moisture significant decreasing trends could be found. Most pronounced trends were observed over Southeast Georgia, implying increasing soil dryness over the area. Based on the fact that surface and mid-troposphere pressure, surface radiation and soil dryness intensified significantly over Western Asia during the last 50 years, it is likely, that Georgia will be exposed to more and longer severe heat waves in future.

Author contributions. I. Keggenhoff performed the analysis and wrote the paper; M. Elizbarashvili assembled and contributed the raw observation data and L. King supervised the project. All authors discussed the results and implications of the manuscript.

Acknowledgements. This study was supported by the research grant International Postgraduate Studies in Water Technologies (IPSWaT) of the International Bureau, Federal Ministry of Education and Research, Germany and the German-Georgian project Amies (Analysing multiple interrelationships between environmental and societal processes in mountainous regions of Georgia) of Volkswagen Stiftung. We highly appreciate the valuable suggestions by the editor and the reviewers to improve our paper. We also thank Nato Kutaladze and the National Environmental Agency of Georgia (NEA) for providing the metadata. We acknowledge also the NOAA/ESRL Physical Sciences Division, Boulder Colorado and the KNMI Climate Explorer for providing data and the SVD analysis tool. Many thanks also go to Alexander Maier for comments and proofreading the manuscript.

ESDD
6, 2273–2322, 2015

References

Arkhipkin, V. S., Gippius, F. N., Koltermann, K. P., and Surkova, G. V.: Wind waves in the Black Sea: results of a hindcast study, Nat. Hazards Earth Syst. Sci., 14, 2883–2897, doi:10.5194/nhess-14-2883-2014, 2014.

Arkhipkin, V. S., Gippius, F. N., Koltermann, K. P., and Surkova, G. V.: Corrigendum to "Wind waves in the Black Sea: results of a hindcast study" published in Nat. Hazards Earth Syst. Sci., 14, 2883–2897, 2014, Nat. Hazards Earth Syst. Sci., 15, 767–767, doi:10.5194/nhess-15-767-2015, 2015.

Baek, K. H., Kim, J., Park, R., Chance, K., and Kurosu, T.: Validation of OMI HCHO data and its analysis over Asia, Sci. Total Environ., 490, 93–105, 2014.

Barnett, T. P. and Preisendorfer, R. W.: Origins and levels of monthly and seasonal forecast skill for United States surface air temperatures determined by canonical correlation analysis, Mon. Weather Rev., 115, 1825–1850, 1987.

Barriopedro, D., Fischer, E. M., Luterbacher, J., Trigo, R. M., and García-Herrera, R.: The hot summer of 2010: redrawing the temperature record map of Europe, Science, 332, 220–224, 2011.

Basu, R. and Samet, J. M.: Relation between elevated ambient temperature and mortality: a review of the epidemiologic evidence, Epidemiol. Rev., 24, 190–202, 2002.

Beniston, M. and Stephenson, D. B.: Extreme climatic events and their evolution under changing climatic conditions, Global Planet. Change, 44, 1–9, 2004.

Black, E. and Sutton, R.: The influence of oceanic conditions on the European summer of 2003, Clim. Dynam., 28, 53–66, 2007.

Black, E., Blackburn, M., Harrison, G., Hoskins, B., and Methven, J.: Factors contributing to the summer 2003 European heatwave, Weather, 59, 217–223, 2004.

Bretherton, C. S., Smith, C., and Wallace, J. M.: An intercomparison of methods for finding coupled patterns in climate data, J. Climate, 5, 541–560, 1992.

Buzzi, A. and Tibaldi, S.: Cyclogenesis on the lee of alps: a case study, Q. J. Roy. Meteorol. Soc., 104, 1542–1566, 1978.

Carril, A. F., Gualdi, S., Cherchi, A., and Navarra, A.: Heatwaves in Europe: areas of homogeneous variability and links with the regional to large-scale atmospheric and SSTs anomalies, Clim. Dynam., 30, 77–98, 2008.

ESDD
6, 2273–2322, 2015

Cassou, C., Terray, L., and Phillips, A. S.: Tropical Atlantic influence on European heat waves, J. Climate, 18, 2805–2811, 2005.
Changnon, S. A., Kunkel, K. E., and Reinke, B. C.: Impacts and responses to the 1995 heat wave: a call to action, B. Am. Meteorol. Soc., 77, 1497–1506, 1996.
Cherry, S.: Singular value decomposition analysis and canonical correlation analysis, J. Climate, 9, 2003–2009, 1996.
Christidis, N., Stott, P. A., and Brown, S. J.: The role of human activity in the recent warming of extremely warm daytime temperatures, J. Climate, 24, 1922–1930, 2011.
Christidis, N., Stott, P. A., Jones, G. S., Shiogama, H., Nozawa, T., and Luterbacher, J.: Human activity and anomalously warm seasons in Europe, Int. J. Climatol., 32, 225–239, 2012.
Collins, D. A., Della-Marta, P. M., Plummer, N., and Trewin, B. C.: Trends in annual frequencies of extremes temperature events in Australia, Aust. Meteorol. Mag., 49, 277–292, 2000.
de Vries, A. J., Tyrlis, E., Edry, D., Krichak, S. O., Steil, B., and Lelieveld, J.: Extreme precipitation events in the Middle East: dynamics of the Active Red Sea Trough, J. Geophys. Res.-Atmos., 118, 7087–7108, 2013.
Della-Marta, P. M., Luterbacher, J., von Weissenfluh, H., Xoplaki, E., Brunet, M., and Wanner, H.: Summer heat waves over western Europe 1880–2003, their relationship to large-scale forcings and predictability, Clim. Dynam., 29, 251–275, 2007.
Dole, R., Hoerling, M., Perlwitz, J., Eischeid, J., Pegion, P., Zhang, T., Quan, X.-W., Xu, T., and Murray, D.: Was there a basis for anticipating the 2010 Russian heat wave?, Geophys. Res. Lett., 38, L06702, doi:10.1029/2010GL046582, 2011.
Ferranti, L. and Viterbo, P.: The European summer of 2003: sensitivity to soil water initial conditions, J. Climate, 19, 3659–3680, 2006.
Feudale, L. and Shukla, J.: Influence of sea surface temperature on the European heat wave of 2003 summer, Part I: An observational study, Clim. Dynam., 36, 1691–1703, 2011a.
Feudale, L. and Shukla, J.: Influence of sea surface temperature on the European heat wave of 2003 summer, Part II: A modeling study, Clim. Dynam., 36, 1705–1715, 2011b.
Fink, A., Brucher, T., Kruger, A., Leckebush, G., Pinto, J., and Ulbrich, U.: The 2003 European summer heatwaves and drought-synoptic diagnosis and impacts, Weather, 59, 209–216, 2004.
Fischer, E. M., Seneviratne, S. I., Luthi, D., and Schär, C.: Contribution of land–atmosphere coupling to recent European summer heat waves, Geophys. Res. Lett., 34, L06707, doi:10.1029/2006GL029068, 2007.

ESDD
6, 2273–2322, 2015

Grumm, R. H.: The central European and Russian heat event of July–August 2010, B. Am. Meteorol. Soc., 92, 1285–1296, 2011.
Haarsma, R. J., Selten, F., van den Hurk, B., Hazeleger, W., and Wang, X.: Drier Mediterranean soils due to greenhouse warming bring easterly winds over summertime central Europe, Geophys. Res. Lett., 36, L04705, doi:10.1029/2008GL036617, 2009.
Haylock, M. and Goodess, C.: Interannual variability of European extreme winter rainfall and links with mean large-scale circulation, Int. J. Climatol., 24, 759–776, 2004.
Hirschi, M., Seneviratne, S. I., Alexandrov, V., Boberg, F., Boroneant, C., Christensen, O. B., Formayer, H., Orlowsky, B., and Stepanek, P.: Observational evidence for soil-moisture impact on hot extremes in southeastern Europe, Nat. Geosci., 4, 17–21, 2011.
IPCC: Climate Change 2014: Impacts, Adaptation, and Vulnerability, Part B: Regional Aspects, in: Contribution of Working Group II to the Fifth Assessment Report of the Intergovernmental Panel on Climate Change, edited by: Barros, V. R., Field, C. B., Dokken, D. J., Mastrandrea, M. D., Mach, K. J., Bilir, T. E., Chatterjee, M., Ebi, K. L., Estrada, Y. O., Genova, R. C., Girma, B., Kissel, E. S., Levy, A. N., MacCracken, S., Mastrandrea, P. R., and White, L. L., Cambridge University Press, Cambridge, UK, New York, NY, USA, 688 pp., 2014.
Jäger, E. B. and Seneviratne, S. I.: Impact of soil moisture-atmosphere coupling on European climate extremes and trends in a regional climate model, Clim. Dynam., 36, 1919–1939, 2011.
Jones, G. S., Stott, P. A., and Christidis, N.: Human contribution to rapidly increasing frequency of very warm Northern Hemisphere summers, J. Geophys. Res., 113, 2156–2202, 2008.
Jung, T., Ferranti, L., and Tompkins, A. M.: Response to the summer 2003 Mediterranean SST anomalies over Europe and Africa, J. Climate, 19, 5439–5454, 2006.
Kalnay, E. M., Kanamitsu, M., Kistler, R., Collins, W., Deaven, D., Gandin, L., Iredell, M., White, G., Woolen, J., Zhu, Y., Chelliah, M., Ebisuzaki, W., Higgins, W., Janowiak, J., Mo, K., and Joseph, D.: The NCEP/NCAR 40-year reanalysis project, B. Am. Meteorol. Soc., 77, 437–471, 1996.
Keggenhoff, I., Elizbarashvili, M., Amiri-Farahani, A., and King, L.: Trends in daily temperature and precipitation extremes over Georgia, 1971–2010, Weather Clim. Ext., 4, 75–85, 2014.
Keggenhoff, I., Elizbarashvili, M., and King, L.: Recent changes in Georgia's temperature means and extremes: annual and seasonal trends between 1961 and 2010, Weather Clim. Ext., 8, 34–45, 2015a.

ESDD
6, 2273–2322, 2015

Keggenhoff, I., Elizbarashvili, M., and King, L.: Heat wave events over Georgia since 1961: climatology, changes and severity, Climate, 3, 308–328, 2015b.
Kendall, M. G.: Rank Correlation Methods, Charles Griffin, London, UK, 1975.
Kostianoy, A. G. and Kosarev, A. N.: The Black Sea Environment, Springer, Berlin, Heidelberg, Germany, 2008.
Kuglitsch, F. G., Toreti, A., Xoplaki, E., Della-Marta, P. M., Zerefos, C. S., Türkeş, M., and Luterbacher, J.: Heat wave changes in the eastern Mediterranean since 1960, Geophys. Res. Lett., 37, L04802, doi:10.1029/2009GL041841, 2010.
Langlois, N., Herbst, J., Mason, K., Nairn, J., and Byard, R. W.: Using the Excess Heat Factor (EHF) to predict the risk of heat related deaths, J. Forens. Legal Med., 20, 408–411, 2013.
Lelieveld, J., Hadjinicolaou, P., Kostopoulou, E., Chenoweth, J., El Maayar, M., Giannakopoulos, C., Hannides, C., Lange, M. A., Tanarhte, M., Tyrlis, E., and Xoplaki, E.: Climate change and impacts in the Eastern Mediterranean and the Middle East, Climatic Change, 114, 667–687, 2012.
Lelieveld, J., Hadjinicolaou, P., Kostopoulou, E., Giannakopoulos, C., Tanarhte, M., and Tyrlis, E.: Model projected heat extremes and air pollution in the eastern Mediterranean and Middle East in the twenty-first century, Reg. Environ. Change, 14, 1937–1949, 2013.
Luterbacher, J., Koenig, S. J., Franke, J., van der Schrier, G., Zorita, E., Moberg, A., Jacobeit, J., Della-Marta, P. M., Küttel, M., Xoplaki, E., Wheeler, D., Rutishauer, T., Stössel, M., Wanner, H., Brázdil, R., Dobrovolný, P., Camuffo, D., Bertolin, C., van Engelen, A., Gonzalez-Rouco, F. J., Wilson, R., Pfister, C., Limanówka, D., Nordli, Ø., Leijonhufvud, L., Söderberg, J., Allan, R., Barriendos, M., Glaser, R., Riemann, D., Hao, Z., and Zerefos, C. S.: Circulation dynamics and its influence on European and Mediterranean January–April climate over the past half millennium: results and insights from instrumental data, documentary evidence and coupled climate models, Climatic Change, 101, 201–234, 2009.
Mann, H. B.: Non-parametric tests against trend, Econometrica, 13, 245–259, 1945.
McBride, J. L., Mills, G. A., and Wain, A. G.: The Meteorology of Australian Heatwaves, Understanding High Impact Weather, CAWCR Modelling Workshop, 30 November–2 December 2009, Melbourne, Australia, 2009.
Meehl, G. A. and Tebaldi, C.: More intense, more frequent, and longer lasting heat waves in the 21st century, Science, 305, 994–997, 2004.

ESDD
6, 2273–2322, 2015

Mo, R. and Straus, D. M.: Statistical-dynamical seasonal prediction based on principal component regression of GCM ensemble integrations, Mon. Weather Rev., 130, 2167–2187, 2002.
Müller, B. and Seneviratne, S. I.: Hot days induced by precipitation deficits at the global scale, P. Natl. Acad. Sci. USA, 109, 12398–12403, 2012.
Nairn, J.: Heatwave defined as a heat impact event for all community and business sectors in Australia, extended abstract, 19th International Biometeorology Congress, 4–8 December 2011, University of Auckland, Auckland, New Zealand, 2011.
Nairn, J. and Fawcett, R.: Defining heatwaves: heatwave defined as a heat-impact event servicing all community and business sectors in Australia, CAWCR Technical Report No. 060, CSIRO and Australian Bureau of Meteorology, Adelaide, Australia, 96 pp., 2013.
Nairn, J., Fawcett, R., and Robert, J. B.: The excess heat factor: a metric for heatwave intensity and its use in classifying heatwave severity, Int. J. Environ. Res. Public Health, 12, 227–253, 2015.
Nicholls, N., Skinner, C., Loughnan, M., and Tapper, N.: A simple heat alert system for Melbourne, Australia, Int. J. Biometeorol., 52, 375–384, 2008.
Ogi, M., Yamazaki, K., and Tachibana, Y.: The summer northern annular mode and abnormal summer weather in 2003, Geophys. Res. Lett., 32, L04706, doi:10.1029/2004GL021528, 2005.
Pattenden, S., Nikiforov, B., and Armstrong, B. G.: Mortality and temperature in Sofia and London, J. Epidemiol. Commun. H., 57, 628–633, 2003.
Perkins, S. and Alexander, L.: On the measurement of heat waves, J. Climate, 26, 4500–4517, 2013.
Perkins, S., Alexander, L., and Nairn, J.: Increasing frequency, intensity and duration of observed global heat waves and warm spells, Geophys. Res. Lett., 39, L20714, doi:10.1029/2012GL053361, 2012.
Pezza, A. B., van Rensch, P., and Cai, W.: Severe heat waves in southern Australia: synoptic climatology and large scale connections, Clim. Dynam., 38, 209–224, 2012.
Pfahl, S. and Wernli, H.: Quantifying the relevance of atmospheric blocking for co-located temperature extremes in the Northern Hemisphere on (sub-)daily time scales, Geophys. Res. Lett., 39, L12807, doi:10.1029/2012GL052261, 2012.
Quesada, B., Vautard, R., Yiou, P., Hirschi, M., and Seneviratne, S. I.: Asymmetric European summer heat predictability from wet and dry southern winters and springs, Nat. Clim. Change, 2, 736–741, 2012.

ESDD
6, 2273–2322, 2015

Rowell, D. P.: The impact of Mediterranean SSTs on the Sahelian rainfall season, J. Climate, 16, 849–862, 2003.
Semenza, J. C., Rubin, C. H., Falter, K. H., Selanikio, J. D., Flanders, W. D., Howe, H. L., and Wilhelm, J. L.: Heat-related deaths during the July 1995 heat wave in Chicago, New Engl. J. Med., 335, 84–90, 1996.
Sen, P. K.: Estimates of regression coefficient based on Kendall's tau, J. Am. Stat. Assoc., 63, 1379–1389, 1968.
Seneviratne, S. I., Corti, T., Davin, E. L., Hirschi, M., Jaeger, E. B., Lehner, I. Orlowsky, B., and Teuling, A. J.: Investigating soil moisture–climate interactions in a changing climate: a review, Earth.-Sci. Rev., 99, 125–161, 2010.
Shahgedanova, M.: Climate at present and in the historical past, in: The Physical Geography of Northern Eurasia: Russia and Neighbouring States, edited by: Shahgedanova, M., Oxford University Press, Oxford, UK, 70–102, 2002.
Stott, P., Stone, D., and Allen, M.: Human contribution to the European heatwave of 2003, Nature, 432, 610–614, 2004.
Stefanon, M., D'Andrea, F., and Drobinski, P.: Heatwave classification over Europe and the Mediterranean region, Environ. Res. Lett., 7, 014023, doi:10.1088/1748-9326/7/1/014023, 2012.
Stefanon, M., Drobinski, P., D'Andrea, F., Lebeaupin-Brossier, C., and Bastin, S.: Soil moisture temperature feedbacks at meso-scale during summer heat waves over western Europe, Clim. Dynam., 42, 1309–1324, 2013.
Trigo, R., Garia-Herrera, R., Diaz, J., Trigo, I., and Valente, M.: How exceptional was the early August 2003 heatwave in France?, Geophys. Res. Lett., 32, L10701, doi:10.1029/2005GL022410, 2005.
United Nations, Department of Economic and Social Affairs, Population Division World Population Prospects: the 2011 Revision, available at: http://esa.un.org/unpd/wup/index.htm, last access: 15 October 2015.
Wang, X. L.: A Quantile Matching Adjustment Algorithm for Gaussian Data Series, available at: http://etccdi.pacificclimate.org/RHtest/QMadj_Gaussian.pdf, last access: 15 October 2015.
Wang, X. L. and Feng, Y.: RHtestsV3, User Manual, Environment Canada, Ottawa, Canada, 2010.
Xoplaki, E., Gonzalez-Rouco, F. J., Gyalistras, D., Luterbacher, J., Rickli, R., and Wanner, H.: Interannual summer air temperature variability over Greece and its connection to the large-

ESDD
6, 2273–2322, 2015

scale atmospheric circulation and Mediterranean SSTs 1950–1999, Clim. Dynam., 20, 523–536, 2003a.
Xoplaki, E., Gonzalez-Rouco, J., Luterbacher, J., and Wanner, H.: Mediterranean summer air temperature variability and its connection to the large-scale atmospheric circulation and SSTs, Clim. Dynam., 20, 723–739, 2003b.
Zampieri, M., D'Andrea, F., Vautard, R., Ciais, P., de Noblet-Ducoudré, N., and Yiou, P.: Hot European summers and the role of soil moisture in the propagation of Mediterranean drought, J. Climate, 22, 4747–4758, 2009.
Zittis, G., Hadjinicolaou, P., and Lelieveld, J.: Role of soil moisture in the amplification of climate warming in the Eastern Mediterranean and the Middle East, Clim. Res., 59, 27–37, 2014.
Ziv, B., Saaroni, H., and Alpert, P.: The factors governing the summer regime of the eastern Mediterranean, Int. J. Climatol., 24, 1859–1871, 2004.

ESDD
6, 2273–2322, 2015

Table 1. The 10 most severe heat waves over Georgia between 1961 and 2010. Heat waves are characterized by their year of occurrence, rank, date of the peak EHF (Date), duration (days), intensity ($^{\circ}C^2$) and accumulated heat load ($^{\circ}C^2$).

Year	Rank	Date of Peak EHF	EHF event duration (days)	Heat load ($^{\circ}C^2$)	Acc. heat load ($^{\circ}C^2$)
1966	9	7 Jun	5	10.8	55
		27 Jul	5	5.0	25
1969	6	9 Jun	7	9.9	70
1995	5	24 May	8	10.3	81
1998		6 May	3	10.7	33
	3	22 Jun	14	8.4	114
		31 Jul	5	3.5	17
		30 Aug	7	6.7	49
		16 Sep	8	3.0	25
2000		22 Jul	7	7.7	52
	8	1 Aug	7	8.5	57
2001		15 Jun	1	12.2	17
	4	24 Jul	15	6.3	94
		14 Aug	4	3.8	15
2006		5 Jun	5	6.0	32
	2	14 Aug	18	7.1	127
	7	29 Aug	14	4.3	61
2007	1	28 May	10	20.0	200
		1 Aug	5	4.0	21
		13 Aug	6	2.9	18
		6 Sep	9	2.3	21
2010		6 Jun	4	11.0	47
		15 Jun	6	5.6	35
	10	12 Jul	12	4.6	55
		2 Aug	13	4.0	50
		2 Sep	9	2.3	20

ESDD
6, 2273–2322, 2015

Table 2. Annual Georgia-averaged trends for heat wave aspects HWN, HWD, HWF, HWex between 1961 and 2010 with respective confidence intervals (95 %). Trends significant at the 5 % level are indicated in bold.

Heat wave aspect	Climatology (1961–1990)	Trend magnitude/decade (1961–2010)	Trend magnitude/decade (1981–2010)
Heat Wave Number (no. of events)	1.7	**0.4 (0.2 to 0.6)**	**0.8 (0.5 to 1.3)**
Heat Wave Duration (days)	5.5	**0.9 (0.5 to 1.5)**	**1.8 (0.5 to 3.6)**
Heat Wave Frequency (days)	10.4	**2.9 (1.5 to 4.7)**	**6.6 (2.7 to 10.7)**
Extreme Heat Wave Days (days)	0.3	**0.05 (0.00 to 0.17)**	0.15 (0.00 to 0.60)

ESDD
6, 2273–2322, 2015

Table 3. Changes in the heat wave predictand and predictors averaged over Georgia between 1961 and 2010. Trends significant at the 5 % level are indicated in bold. Respective confidence intervals (95 %) are set in brackets. Reanalysis data focus on an area between 38.8 to 47.8° E and 38.8 to 43.8° N, except for the Black Sea (24 to 42° E and 40 to 47° N) and Caspian Sea (47 to 55° E and 36 to 47° N).

Heat wave predictand*/ predictors	Climatology (1961–1990)	Mean Difference (1981–2010)	Trend magnitude/decade (1961–2010)	Trend magnitude/decade (1981–2010)
*Tmean95p (°C)	20.4	0.1	0.2 (0.0 to 0.4)	**0.4 (0.0 to 0.9)**
SST (Caspian Sea) (°C)	21.7*	–	–	**0.7 (0.4 to 1.0)**
SST (Black Sea) (°C)	20.7*	–	–	**0.6 (0.4 to 0.8)**
SLP (mb)	1012	1.2	**0.5 (0.3 to 0.7)**	0.0 (−0.3 to 0.3)
Z500 (m)	5753	15.9	**8.7 (5.4 to 11.1)**	2.3 (−1.4 to 9.2)
u-wind ($m\,s^{-1}$)	6.8	0.6	0.25 (0.0 to 0.6)	−0.4 (−0.1 to 0.12)
v-wind ($m\,s^{-1}$)	3.7	−0.5	**− 0.2 (−0.4 to 0.0)**	0.0 (−0.5 to 0.4)
Outgoing Longwave Radiation ($W\,m^{-2}$)	246	5.8	**2.9 (1.7 to 4.0)**	3.1 (0.6 to 5.4)
Vertical Velocity at 500 mb ($Pa\,s^{-1}$)	−0.04	0.01	**0.01 (0.00 to 0.01)**	0.02 (0.00 to 0.03)
Relative Humidity at 500 mb (%)	44	−4.8	**− 2.4 (−3.2 to −1.5)**	−3.7 (−5.5 to −2.0)
Precipitation ($mm\,day^{-1}$)	5	−0.7	**− 0.35 (−0.47 to −0.23)**	−0.58 (−0.95 to −0.28)
Soil Moisture (fraction)	0.3	−0.01	**− 0.004 (0.006 to 0.002)**	−0.007 (0.012 to 0.002)

* Due to data availability only climatological values and trends for the period 1981–2010 could be presented.

ESDD
6, 2273–2322, 2015

Table 4. Results of the CCAs between selected predictors and the heat wave predictand: listed are the predictor's abbreviation, the selected domain, *r* is the correlation coefficient between the canonical score series, the explained variance refers to the variance of summer heat waves HWs explained by each CCA, the correlation skill score of all grid points with an approximate 95 % confidence interval.

Predictor	Domain	*r*	Explained Variance (%)	Confidence Interval (95 %)
SST (Eurasia)	10–80° N, 0–90° E	0.56	52.3 %	0.43–0.66
SST (Black Sea)	40–47° N, 27–42° E	0.43	88.3 %	0.27–0.59
SST (Caspian Sea)	36–47° N, 47–55° E	0.66	88.6 %	0.55–0.75
Z500	10–80° N, 0–90° E	0.74	61.6 %	0.67–0.80
SLP	10–80° N, 0–90° E	0.62	61.2 %	0.50–0.71
u-wind500	10–80° N, 0–90° E	−0.77	59.4 %	−0.83–−0.70
v-wind500	10–80° N, 0–90° E	0.76	62.4 %	0.70–0.82
O500	10–80° N, 0–90° E	0.81	55.5 %	0.74–0.87
RH500	10–80° N, 0–90° E	0.78	52.1 %	0.71–0.82
OLR	10–80° N, 0–90° E	0.81	51.0 %	0.75–0.85
RR	10–80° N, 0–90° E	−0.84	51.2 %	−0.87–−0.78
SM	10–80° N, 0–90° E	−0.76	50.0 %	−0.81–−0.70

ESDD
6, 2273–2322, 2015

Table A1. Extreme summer heat wave events between 1961 and 2010: Year, HW number, Intensity of peak heat wave (HW class), date of peak EHF (Date), duration (days), accumulated heat load (°C^2), and accumulated heat load (°C^2) of peak extreme heat waves.

Year	HW No.	Date	Peak Intensity (HW class)	Duration (EHF days)	Distribution (% of stations)
1961	1	5 May	4	4	27
	2	15 May	4	5	18
1966	3	7 Jun	4	7	29
1967	4	24 May	4	3	9
1980	5	14 Jul	4	5	5
1996	6	17 Jul	4	14	6
1998	7	7 May	4	4	15
1999	8	6 Aug	4	8	124
2000	9	17 Jul	4	9	11
	10	2 Aug	4	7	24
2001	11	15 Jun	5	5	6
2003	12	26 May	5	4	5
2005	13	22 May	4	3	5
2007	14	9 May	6	3	13
	15	28 May	6	6	75
2009	16	5 Jun	4	4	13

ESDD
6, 2273–2322, 2015

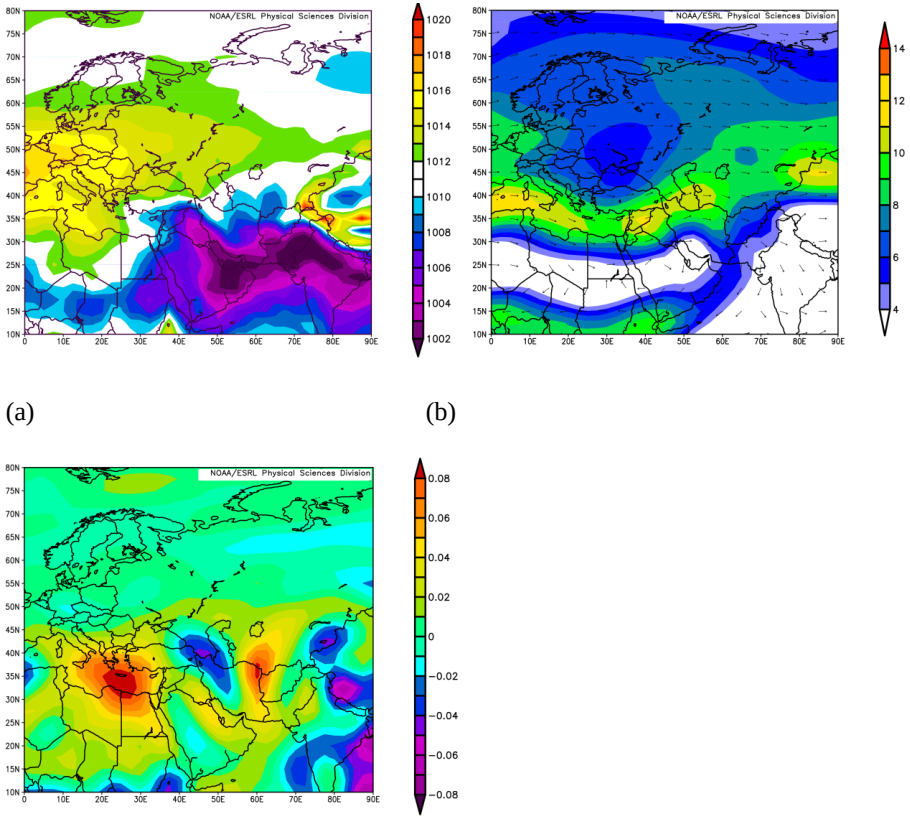

Figure 1. Averaged atmospheric patterns over Eurasia during summer 1981 to 2010: composite means for summer. **(a)** Sea Level Pressure (mb) **(b)** Vector Wind (VW500, $m\,s^{-1}$), and **(c)** Vertical Velocity ($Pa\,s^{-1}$).

ESDD
6, 2273–2322, 2015

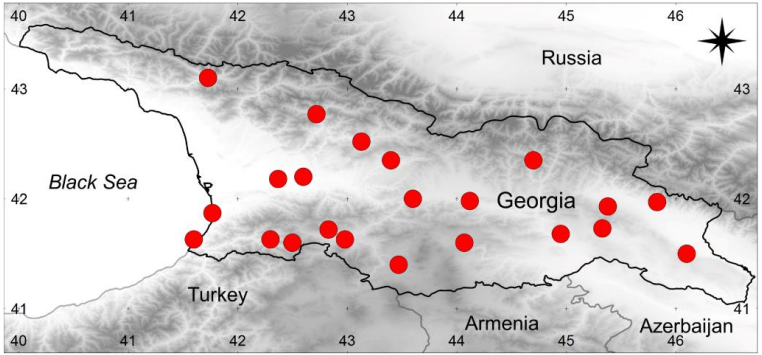

Figure 2. Temperature stations over Georgia used in this study.

ESDD
6, 2273–2322, 2015

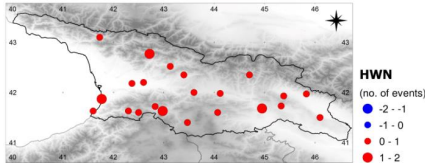

(a)

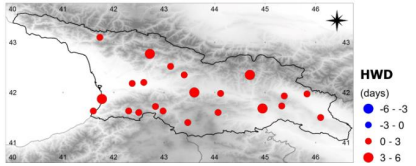

(b)

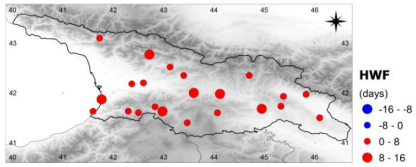

(c)

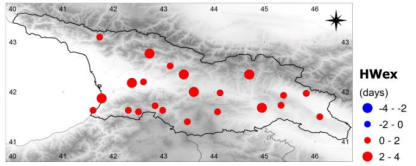

(d)

Figure 3. Absolute heat wave changes between 1961 and 2010 over Georgia: mean absolute differences between the periods 1961–1990 and 1981–2010 for the **(a)** Heat Wave Number (HWN) in number of events, **(b)** Heat Wave Duration (HWD) in days, **(c)** Heat Wave Frequency (HWF) in days and **(d)** Extreme Heat Wave days in days.

ESDD
6, 2273–2322, 2015

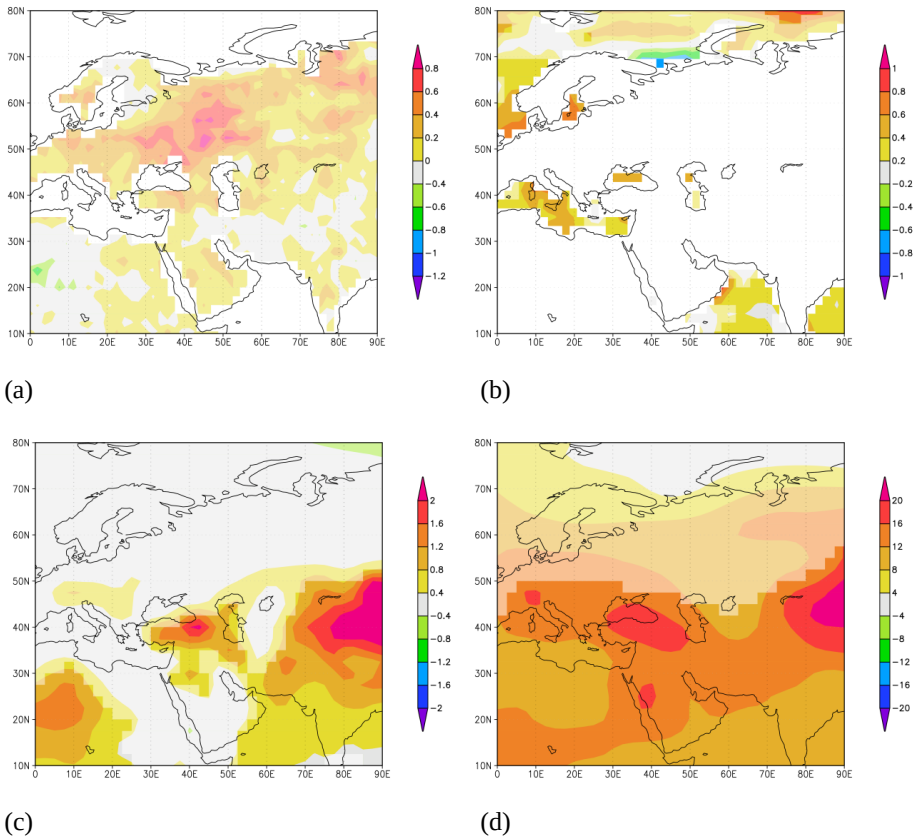

Figure 4. Changes in the heat wave predictand and large-scale circulation over Eurasia between 1961 and 2010: absolute differences between the periods 1961–1990 and 1981–2010 for **(a)** Tmean95p (°C), **(b)** SST (°C), **(c)** SLP (Pa), and **(b)** Z500 (m). Bright coloured fields indicate significant changes (at the 5 % level). Light coloured fields imply insignificance.

ESDD
6, 2273–2322, 2015

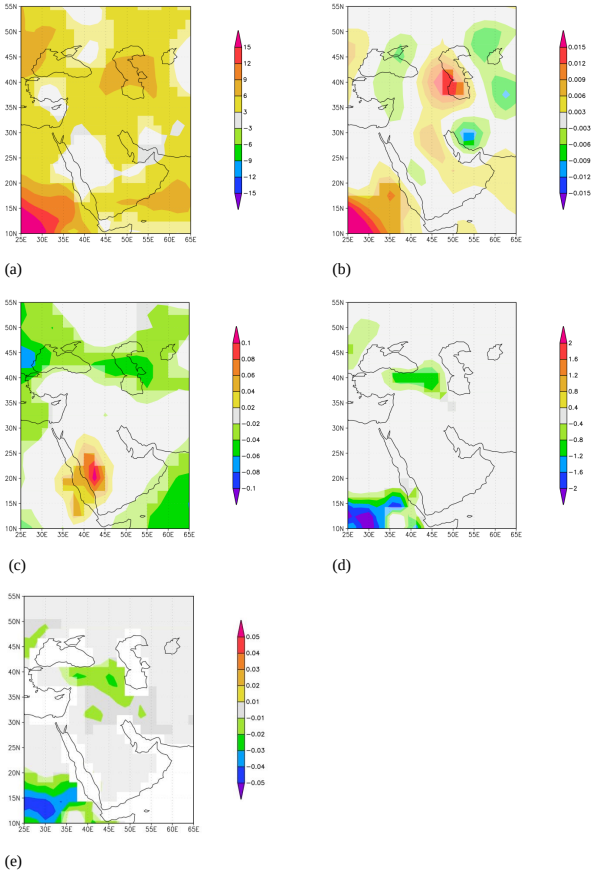

Figure 5. Changes in meso-scale thermal processes between 1961 and 2010 over West Asia: absolute differences between the periods 1961–2010 and 1981–2010 for **(a)** OLR ($W m^{-2}$), **(b)** O500 ($Pa s^{-1}$), **(c)** RH500 (%), **(d)** RR ($mm day^{-1}$), and **(e)** SM (%). Bright coloured fields indicate significant changes (at the 5 % level). Light colored fields imply insignificance.

ESDD
6, 2273–2322, 2015

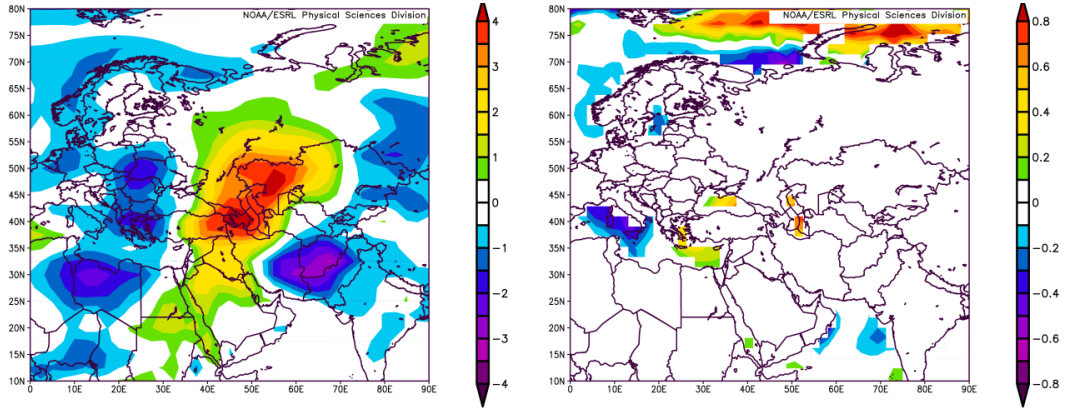

(a) (b)

Figure 6. Composites of SAT and SST during major summer heat waves over Georgia between 1961 and 2010: Composite anomalies for daily **(a)** SAT (°C) and **(b)** SST (°C). Anomalies are calculated with respect to the 1981–2010 period. Data is based on daily NCEP/NCAR Reanalysis.

ESDD
6, 2273–2322, 2015

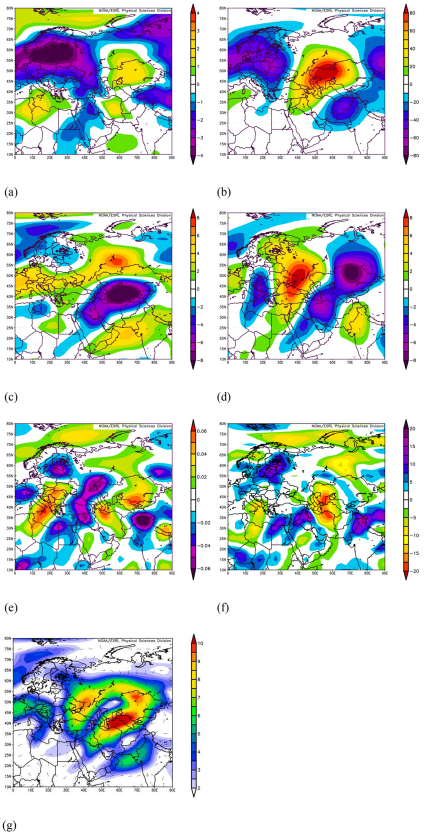

Figure 7. Composites of large-scale circulation and middle troposphere patterns during major summer heat waves over Georgia between 1961 and 2010: Anomalies for daily **(a)** SLP (hPa), **(b)** Z500 (m), **(c)** u-wind at 500 mb ($m\,s^{-1}$), **(d)** v-wind at 500 mb ($m\,s^{-1}$), **(e)** O500 ($Pa\,s^{-1}$), **(f)** RH500 m (%), and **(g)** VW500 ($m\,s^{-1}$). Anomalies are calculated with respect to the 1981–2010 period. Data is based on daily NCEP/NCAR Reanalysis.

ESDD
6, 2273–2322, 2015

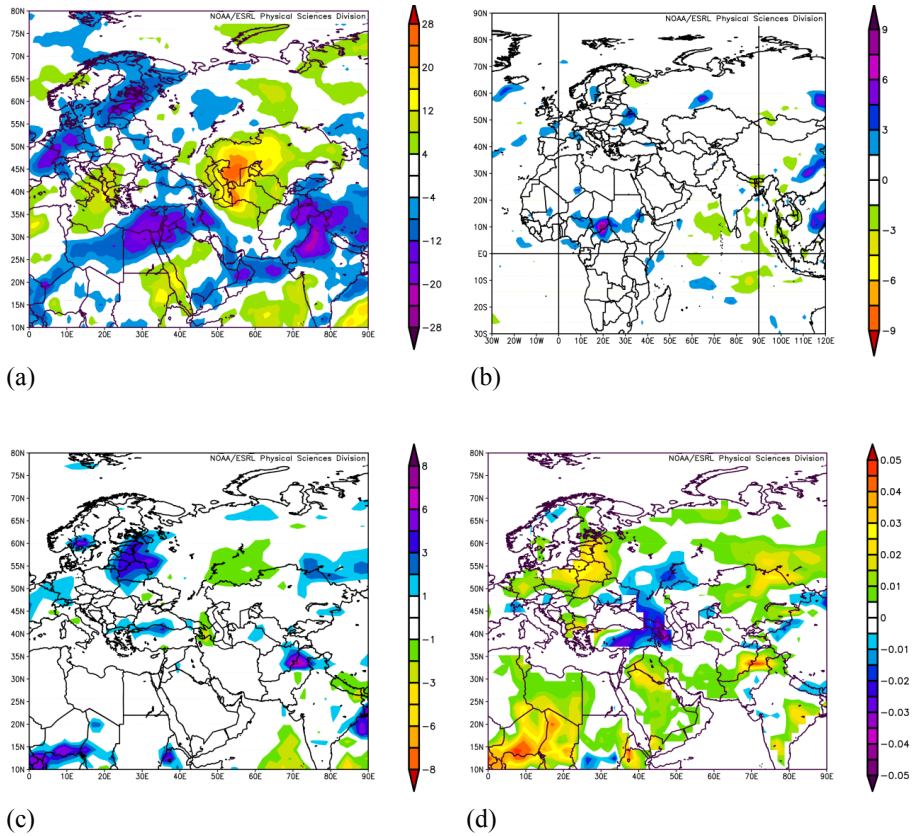

Figure 8. Composites of meso-scale surface patterns during major summer heat waves over Georgia between 1961 and 2010: Anomalies for daily **(a)** OLR ($W m^{-2}$), **(b, c)** RR ($mm day^{-1}$), and **(d)** SM (fraction). Anomalies are calculated with respect to the 1981–2010 period. Data is based on daily NCEP/NCAR Reanalysis.

ESDD
6, 2273–2322, 2015

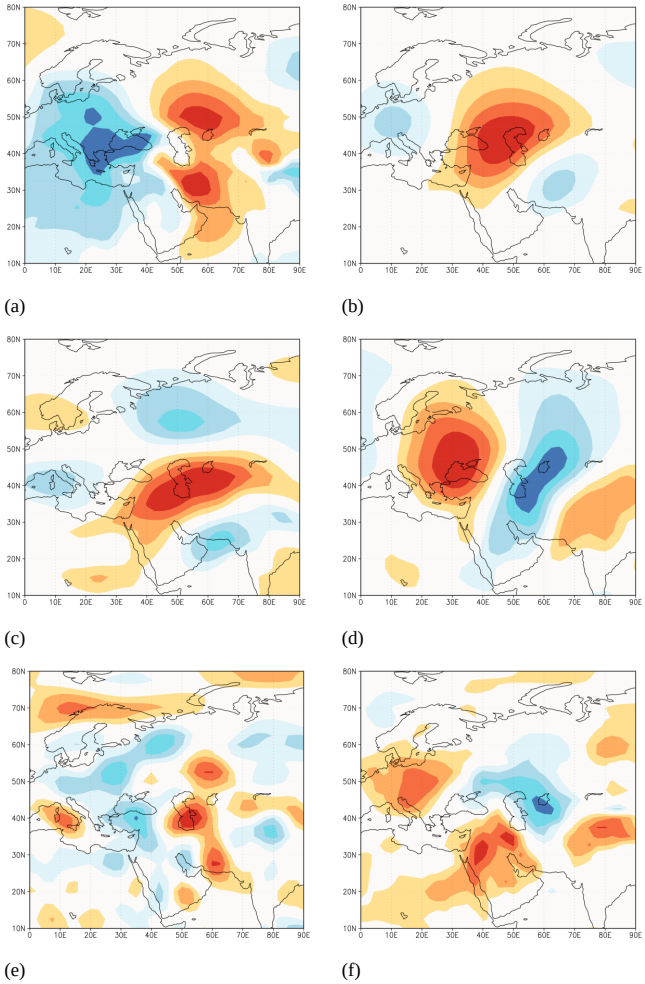

Figure 9.

ESDD
6, 2273–2322, 2015

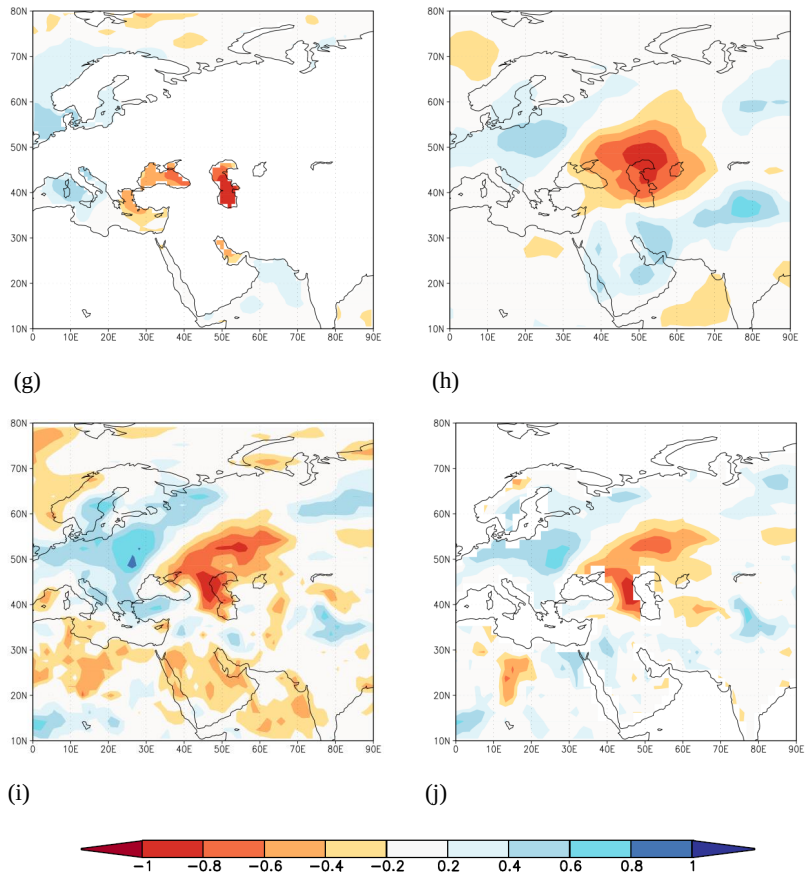

Figure 9. First CCAs between the summer heat wave predictand and selected predictors: CCA modes with the correlation coefficient for **(a)** SLP, **(b)** Z500, **(c)** u-wind at 500 mb, **(d)** v-wind at 500 mb, **(e)** O500, **(f)** RH, **(g)** SST, **(h)** OLR, **(i)** RR, and **(j)** SM. Canonical correlation coefficients are displayed on the top of each panel.

ESDD
6, 2273–2322, 2015